AQUA
Water Infrastructure, Ecosystems and Society

IWA PUBLISHING

 AQUA — Water Infrastructure, Ecosystems and Society Vol 72 No 9, 1800 doi: 10.2166/aqua.2023.313

Sustainable green synthesis of $ZnFe_2O_4$@ZnO nanocomposite using Oleaster tree bark methanolic extract for photocatalytic degradation of aqueous humic acid in the presence of UVc irradiation

Majid Asri[a], Ali Naghizadeh[b,*], Amirhesam Hasani[a], Sobhan Mortazavi-Derazkola[b], Amirhossein Javid[a] and Fatemehsadat Masoudi[c]

[a] Department of Environmental Engineering, Faculty of Natural Research and Environment, Science and Research Branch, Islamic Azad University, Tehran, Iran
[b] Medical Toxicology & Drug Abuse Research Center (MTDRC), Birjand University of Medical Sciences (BUMS), Birjand, Iran
[c] Department of Environmental Health Engineering, Faculty of Health, Shahid Beheshti University of Medical Sciences (SBMU), Tehran, Iran
*Corresponding author. E-mail: al.naghizadeh@yahoo.com

ABSTRACT

One of the most important humic substances in water is humic acid. These substances enter water sources through soils, sediments of aquatic animals, plants and sewage. Therefore, removing them from water sources is very important. In this study, the photocatalytic removal of humic acid was investigated using zinc ferrite nanoparticles loaded with zinc oxide ($ZnFe_2O_4$@ZnO). This research was conducted in an experimental-interventional way in a batch reactor on a laboratory scale. A novel and facile method was applied for catalyst synthesis in different conditions, and it was structurally and morphologically characterized by XRD, FT-IR, SEM, DLS and EDS mapping techniques. The effects of pH (3–11), nanoparticle dose (0.005–0.1 g/L), and humic acid concentration (2–15 mg/L) were examined up to 120 min of time. The results showed that the efficiency of humic acid degradation by $ZnFe_2O_4$@ZnO reached 95% in optimal conditions. Also, it was found that this nanocomposite has an acceptable reusability and recovery after being tested in five stages.

Key words: Advanced oxidation process (AOPs), humic acid, photocatalytic, $ZnFe_2O_4$@ZnO

HIGHLIGHTS

- New magnetic $ZnFe_2O_4$@ZnO nanocomposite was synthesized and characterized.
- FT-IR, SEM, EDS and XRD analyses showed successful synthesis of $ZnFe_2O_4$@ZnO nanocomposite.
- In optimum conditions, 95% degradation efficiency of humic acid was observed.
- Nanocomposite has an acceptable reusability and recovery after being tested in five stages.

GRAPHICAL ABSTRACT

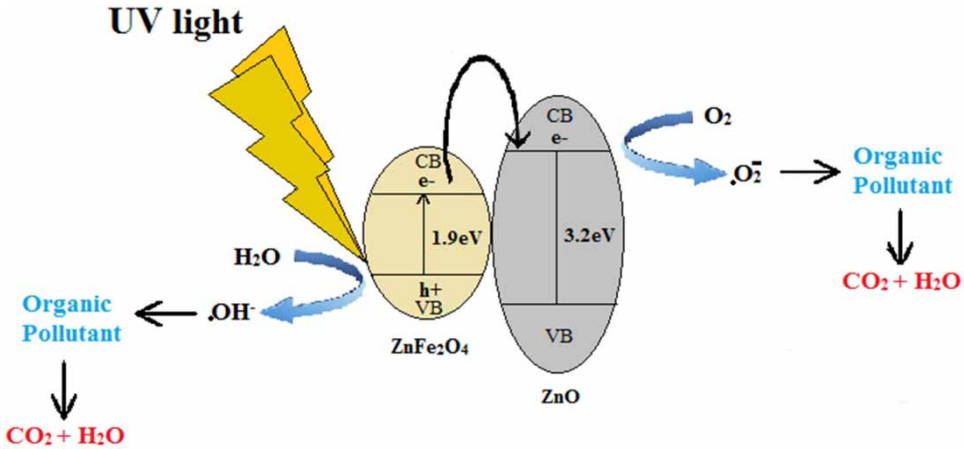

INTRODUCTION

The presence of humic acid in water raises serious concerns due to its ability to form carcinogenic trihalomethanes. It has an adverse effect on the esthetic water quality and may result in biofouling of pipelines with negative hygienic consequences (Naghizadeh *et al.* 2013b; Derakhshani & Naghizadeh 2014). The formation of disinfection byproducts (DBPs) due to the presence of humic compounds in water and acute health problems caused by it has increased the need to pay attention to the use of new methods of removing humic acid in water environments (Naghizadeh *et al.* 2013a; Algamdi *et al.* 2019). In recent years, several methods have been proposed to remove humic acid, such as surface adsorption using activated carbon, ion exchange resins, membrane separation, advanced coagulation, electromicrofiltration and so on. The use of these methods has limitations, such as low removal percentage, high investment and operation cost, lack of easy access, and production of excess sludge and contaminated wastewater, which increases the need for a very efficient and accessible method (Naghizadeh *et al.* 2015; Chianese *et al.* 2020; Tang *et al.* 2020).

Advanced oxidation processes (AOPs) are suitable and high-efficiency methods for purifying water containing pharmaceuticals, biological toxins, dyes, reactive oxygen species and NOMs and converting them into safe products such as carbon dioxide and water (Matilainen & Sillanpää 2010; Amor *et al.* 2019). The AOPs are based on the production of hydroxyl free radicals, which have a very high oxidizing power due to having at least one pair of free electrons. To produce these powerful hydroxyl radicals, ozone, H_2O_2, ultraviolet rays, etc. are used. The combination of these materials leads to the production of hydroxyl radicals with strong oxidizing power to decompose a significant number of organic materials (Sarathy & Mohseni 2006; Stasinakis 2008; Babu *et al.* 2019; Ghernaout & Elboughdiri 2020).

In the photocatalyst process, UV light is used to excite the semiconductor catalyst. In this process, the pollutant is exposed to UV radiation in the presence of photocatalytic particles in the course of surface reaction, in which electrons (e^-) move from the valence band (VB) to the conduction band. As a result, positive holes (h^+) are formed and oxidation and reduction reactions are carried out on the surface of the catalyst (Moctezuma *et al.* 2012).

ZnO is a semiconductor with the characteristics of chemical stability, high activity and environmental friendliness, which is widely used as a catalyst. However, although this semiconductor has excellent photocatalytic activity, due to its wide bandgap (3.2 eV), it causes unfavorable absorption in the visible light region, which reduces its efficiency against visible light. One of the effective solutions to solve this problem is using spill materials with a narrow bandgap such as $ZnFe_2O_4$ (1.9 eV) including favorable photochemical and magnetic stability characteristics and high performance in the visible light region. $ZnFe_2O_4$ alone also has weak photogradation activity. Therefore, it is expected that the combination and synthesis of the p-type semiconductor ($ZnFe_2O_4$) with the n-type semiconductor (Zn) and the $ZnFe_2O_4$@ZnO nanocomposite eventually, access to the surface of the reactants and as a result the photocatalytic process will increase (Sun *et al.* 2013; Rameshbabu *et al.* 2016; Wang *et al.* 2017; Yadav *et al.* 2018; Zouhier *et al.* 2020; Nguyen *et al.* 2022).

There are various physical and chemical methods for the synthesis of nanoparticles. Meanwhile, the method of green synthesis of nanoparticles using microorganisms, enzymes, plants and plant extracts is a compatible, environmentally friendly and cost-effective alternative to physical and chemical methods. This method causes the synthesis of nanoparticles in a wide range and with less contamination compared to other methods. The synthesis of zinc oxide nanoparticles using the green synthesis method shows the stabilization and high stability of nanoparticles (Geoprincy *et al.* 2013; Agarwal *et al.* 2017; Nabi *et al.* 2018).

In this research, the capability of $ZnFe_2O_4$@ZnO nanocomposite synthesized by the green synthesis method for the photocatalytic degradation of humic acid under the influence of UVc was studied. Also, the effects of parameters such as solution pH, contact time, nanoparticle dosage and different concentrations of humic acid were discussed and investigated.

EXPERIMENTAL

Materials and method

All materials used in this study were sourced from Merck Company. The photocatalytic reactor was used in this study on a laboratory scale and in a discontinuous manner. The reactor was a cylinder with a volume of 2 L made of Pyrex material that was equipped with a sampling port, a water circulation system in the outer part of the reactor to cool it, a magnet to stir the sample by placing it on the stirrer and a radiation source (Figure 1). The source of ultraviolet radiation in this study is a UV-C lamp with a power of 18 W, wavelength of 253 nm and a radiation intensity of 294–282 w/m at a distance of 1 cm, which was

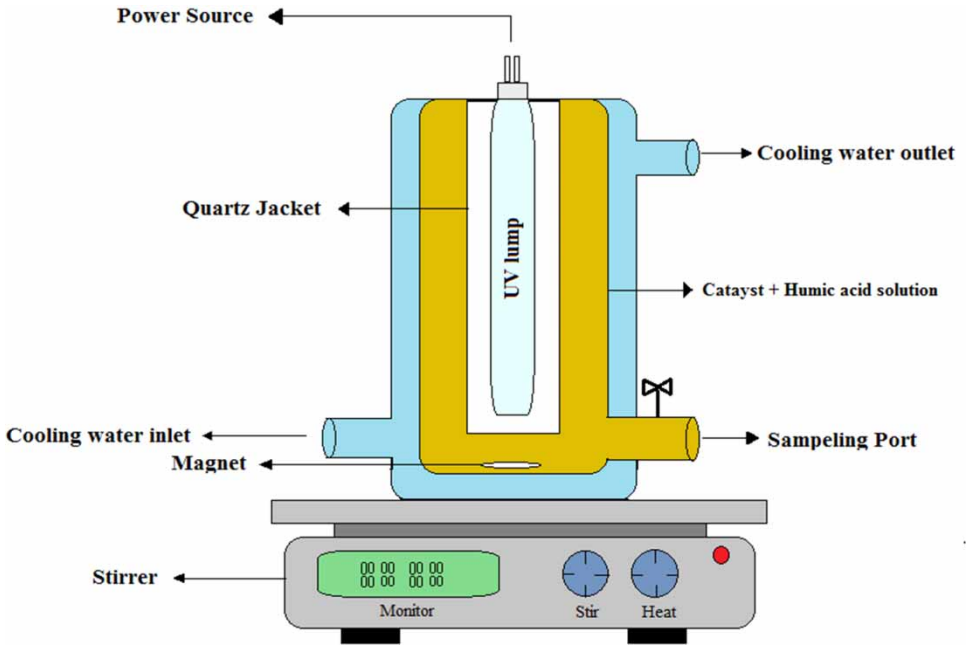

Figure 1 | Schematic of the photocatalytic reactor for degradation of humic acid by $ZnFe_2O_4$@ZnO.

manufactured by Philips, Poland. The lamp was placed inside a very transparent quartz cover along the length of the reactor and in the center of the reactor interior.

In order to investigate the morphology characterization and specific surface of the synthesized nanocomposite, methods such as scanning electron microscopy (SEM) (HITACHI, S4160, Japan), energy-dispersive X-ray spectroscopy (EDS) (Oxford Instruments, United Kingdom), X-ray diffraction (XRD) (Philips, PW1730, Holland), Fourier transform infrared spectroscopy (FT-IR) (Thermo Nicolet, AVATAR, 370 FT-IR, USA) and dynamic light scattering analysis (DLS) (Horiba, Japan) were used.

To determine the zero charge potential of $ZnFe_2O_4$@ZnO nanocomposite, Erlenmeyer flasks containing 50 mL of distilled water at different pH levels and 0.025 g of nanocomposite were prepared. After stirring for 24 h, the final pH was determined.

Various parameters affecting the photocatalytic process such as pH (11–3), nanocomposite concentrations in the range of 0.1–0.005 g/L, different concentrations of humic acid (2–15 mg/L) during the contact time of 10–100 min were studied. At first, after adding the desired materials to the reactor, it was stirred for 30 min in the dark to reach the absorption–desorption equilibrium, and then the solution was exposed to the light of the lamp until the end. At the mentioned time intervals, 5 mL sampling was done and after separating the nanoparticles from the sample solution, it was determined by a spectrophotometer (UV/VIS spectrophotometer T80 + , PG Instrument Ltd, England) at wavelength 290 nm.

The efficiency of humic acid degradation was calculated using the following equation:

$$R = \frac{C_0 - C_e}{C_0} \times 100 \quad (1)$$

where R is equal to the degradation efficiency (%), C_0 and C_e are equal to the initial and final concentrations of humic acid (mg/L), respectively (Kamranifar *et al.* 2019a).

Synthesis of $ZnFe_2O_4$ and $ZnFe_2O_4$@ZnO materials

$ZnFe_2O_4$ nanoparticles were synthesized using previous studies with a slight modification. Typically, 8 g of iron salt ($FeCl_3{\cdot}6H_2O$) was dissolved in 30 mL of degassed deionized water under vigorous stirring. Then, 3.86 g of zinc salt ($Zn(NO_3)_2{\cdot}4H_2O$) was dissolved in 30 mL of deionized water and added to the iron salt solution. In this research, the molar ratio of Fe^{3+}:Mn^{2+} was 2:1. The transparent solutions of zinc and iron were mixed together under vigorous stirring for

45 min. Then, 1 g of Sodium Dodecyle Sulfate (SDS) surfactant dissolved in 30 mL of distilled water was slowly added to the mixture. Then, aqueous sodium hydroxide was added to the above mixture to maintain the pH = 12. After 2 h, the zinc ferrite was synthesized after washing with water and ethanol, drying and calcining at 500 °C for 3 h. Secondly, $ZnFe_2O_4$@ZnO materials were synthesized by the co-precipitation route. First, 0.5 g of obtained $ZnFe_2O_4$ from the previous step was dispersed in 30 mL of deionized water for 30 min. Then, 1.2 g of $Zn(NO_3)_2{\cdot}4H_2O$ was added to the solution under vigorous stirring (pH = 12). The mixture was magnetically stirred for 2 h. Finally, the sample was dried and calcinated to 500 °C for 3 h (Shirzadi-Ahodashti *et al.* 2020; Nguyen *et al.* 2022).

Extraction from Oleaster tree bark and green synthesis $ZnFe_2O_4$@ZnO of nanocomposite

After collecting the Oleaster tree bark and preparing it, extraction was done by percolation method using methanol. At first, after cleaning and washing, the plant was dried and immersed in methanol from the part of the separating funnel and the methanol was drained after a period of 12 h. We continued this process for 72 h (3 days) and then used a rotary apparatus to separate methanol from the ingredients to separate the desired extract.

In a further step, 1 g of the synthesized nanocomposite was mixed with 50 mL of ethanol and distilled water and dispersed under ultrasonic conditions for 30 min. Then, in another container, 6.25 g of $Zn(NO_3)_2{\cdot}6H_2O$ was slowly added to the container containing the $ZnFe_2O_4$ mixture. After 2 h of intense ultrasonic stirring, the final product was centrifuged and washed three times with water and ethanol. Then, to achieve the final product of sediment obtained it was calcined at 350 °C for 2 h (Krishnan *et al.* 2021).

RESULTS AND DISCUSSION

Morphology of $ZnFe_2O_4$ and $ZnFe_2O_4$@ZnO

SEM was used to characterize the surface structure of the sample. The SEM images of the $ZnFe_2O_4$ and $ZnFe_2O_4$@ZnO are illustrated in Figure 2. SEM images of $ZnFe_2O_4$ showed that the as-synthesized products consist of well crystallized homogeneous spherical and oval morphology particle-like nanocrystals, which are agglomerated together, because of the presence of magnetic interactions among the particles. When the ZnO nanoparticles were placed on the surface of the $ZnFe_2O_4$, the size of the nanoparticles increased. As can be seen from SEM image of the ZnO nanoparticles placed on the surface of the $ZnFe_2O_4$, the morphology and uniformity of the nanoparticles changed. Agglomerated particles due to increased magnetic properties can be one of the reasons for this phenomenon (Rabbani *et al.* 2016).

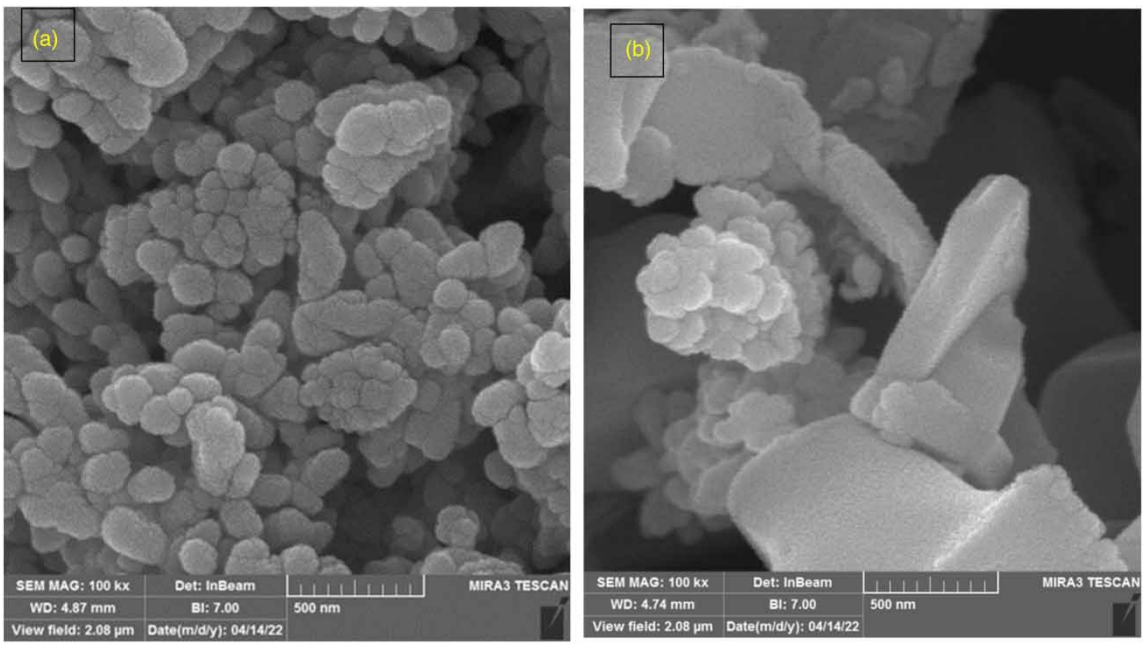

Figure 2 | The SEM images of (a) $ZnFe_2O_4$ and (b) $ZnFe_2O_4$@ZnO.

The EDS analysis was used to determine the elemental composition of the $ZnFe_2O_4$ and $ZnFe_2O_4$@ZnO. As can be seen in Figure 3, an examination of the resulting spectrum confirmed the presence of the zinc (Zn), iron (Fe) and oxygen (O) elements. In addition, EDS elemental mapping of the $ZnFe_2O_4$ nanoparticles also describes the space distribution of Zn, O and Fe elements (Figure 4(a)). This analysis was also performed for $ZnFe_2O_4$-ZnO (Figure 4(b)) samples. The results showed that the elements were evenly distributed.

XRD analysis of $ZnFe_2O_4$ and $ZnFe_2O_4$@ZnO

The crystalline structures of the synthesized materials were further determined by XRD analysis. The XRD patterns of $ZnFe_2O_4$ (a) and $ZnFe_2O_4$@ZnO (b) are shown in Figure 5. For the $ZnFe_2O_4$ nanoparticles, diffraction peaks at $2\theta =$ 29.86°, 35.25°, 42.62°, 56.65° and 62.25° are observed, which correspond to the (220), (311), (400), (511) and (440) planes

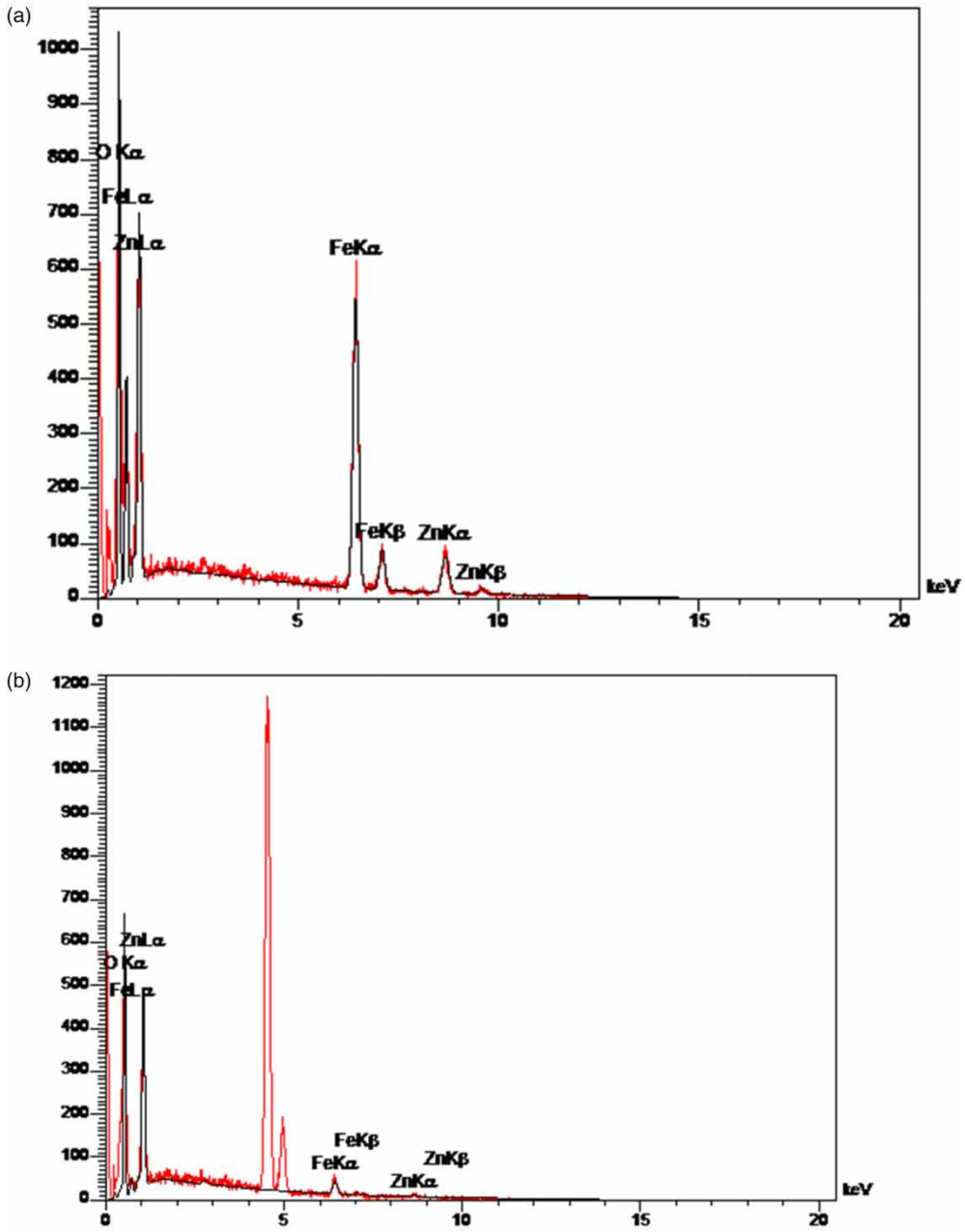

Figure 3 | Energy-dispersive X-ray spectroscopy (EDS) analysis of (a) $ZnFe_2O_4$ and (b) $ZnFe_2O_4$@ZnO.

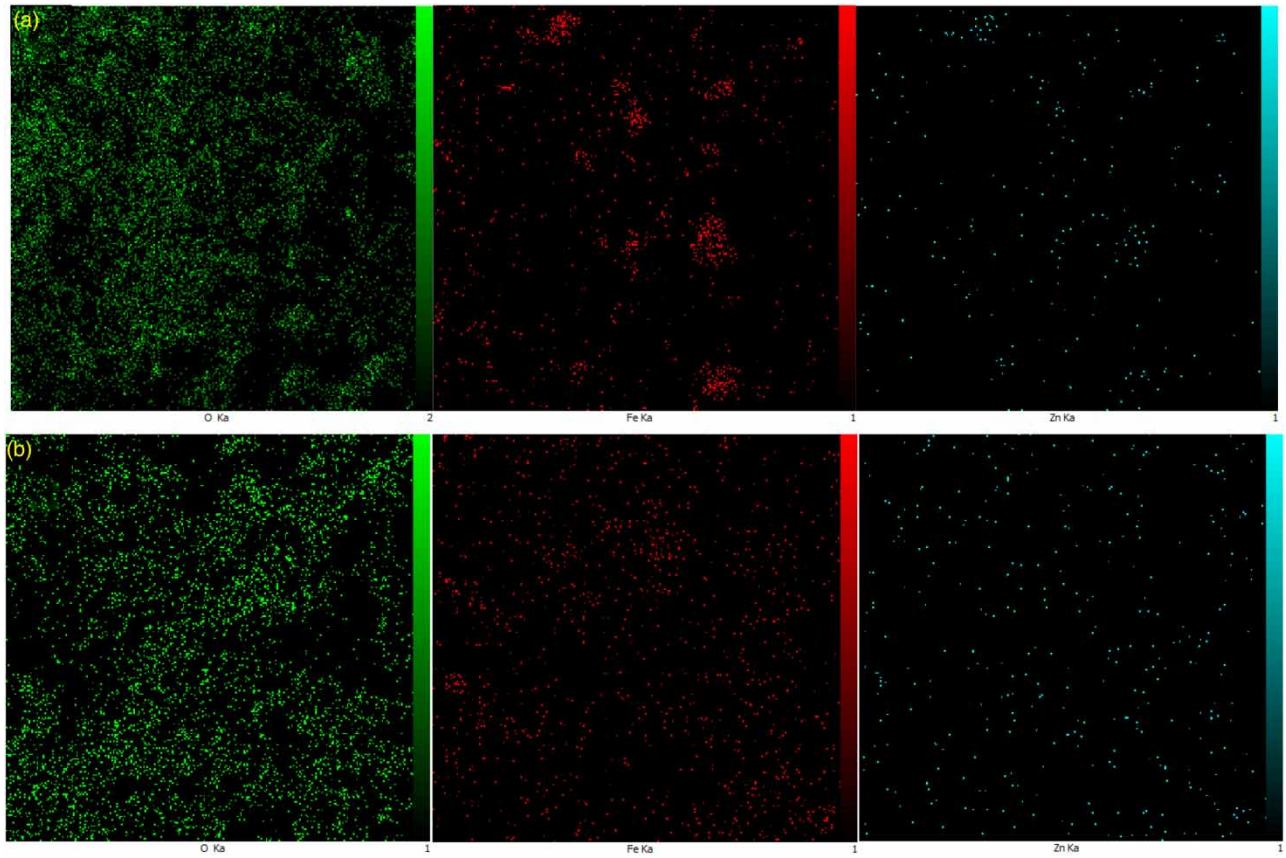

Figure 4 | EDS elemental mapping of (a) $ZnFe_2O_4$ and (b) $ZnFe_2O_4$@ZnO nanoparticles.

of $ZnFe_2O_4$, respectively. All diffraction peaks in the XRD pattern of the as-synthesized magnetic $ZnFe_2O_4$ nanoparticles can be easily indexed with the reported data (JCPDS: 01-089-1012). The XRD pattern of $ZnFe_2O_4$@ZnO exhibited approximately the same feature as $ZnFe_2O_4$, except that a sharp peak centered at 31.9°, 34.5°, 36.3°, 47.6°, 56.7°, 62.9°, 66.4°, 68° and 69.2° of 2θ corresponding to ZnO was observed (Lv *et al.* 2010; Li *et al.* 2018; Su *et al.* 2018).

FT-IR spectra of $ZnFe_2O_4$ and $ZnFe_2O_4$@ZnO

The FT-IR of $ZnFe_2O_4$ and $ZnFe_2O_4$@ZnO nanocomposites are presented in Figure 6. In all spectra, the broad peaks at about 3,400 cm^{-1} and the low intensive peak at about 1,600 cm^{-1} are related to the stretching and bending vibration of water molecules, respectively. Furthermore, an obvious peak at about 760 cm^{-1} is attributed to Zn–O bond vibration (Figure 6(a)). The FT-IR spectrum of $ZnFe_2O_4$@ZnO nanocomposites is shown in Figure 6(b). In a spectrum, the bonding of magnetic materials is observed at a peak of 400–900 cm^{-1} (Zn–O and Fe–O bonds). The band at 1451 is assigned to C–H bending modes (Yadav *et al.* 2018).

DLS analysis and zeta potential of $ZnFe_2O_4$ and $ZnFe_2O_4$@ZnO

The surface charge and distribution of the sizes of $ZnFe_2O_4$ (a) and $ZnFe_2O_4$@ZnO (b) were calculated through zeta potential and DLS (dynamic light scattering) analysis, respectively. The histogram of DLS analysis for the particle size distribution of prepared $ZnFe_2O_4$ (a) and $ZnFe_2O_4$@ZnO (b) is shown in Figure 7. DLS analysis revealed that the average sizes of $ZnFe_2O_4$ and $ZnFe_2O_4$@ZnO were approximately 60–90 nm and 75–200 nm, respectively. In addition, the zeta potential values of synthesized magnetic $ZnFe_2O_4$ and $ZnFe_2O_4$@ZnO were −8.73 and −2.3 mV (Figure 8).

Measurement of zero-point charge

At first, the result of pHzpc determination of the photocatalytic effect of $ZnFe_2O_4$@ZnO nanocomposite is shown in Figure 9. As is clear from the figure, the process of the photocatalytic effect of $ZnFe_2O_4$@ZnO nanocomposite had better conditions

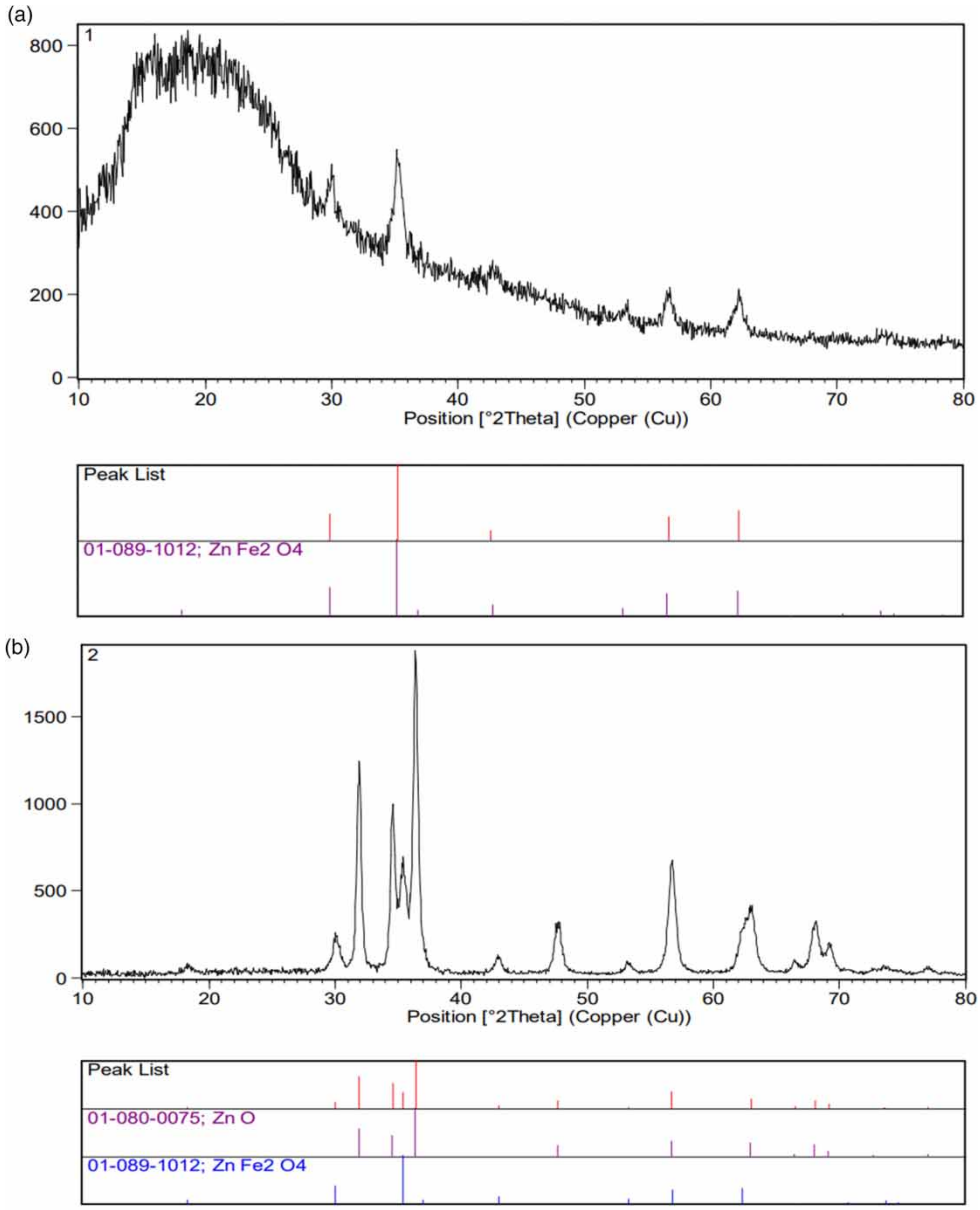

Figure 5 | XRD analysis of (a) $ZnFe_2O_4$ and (b) $ZnFe_2O_4$@ZnO.

under pHzpc = 6.4 conditions. At pH lower than pHzpc, the amount of positive charge density on the surface of the nanocomposite increases and the electrostatic force of attraction between the surface of the positive charge of the nanocomposite and the anionic nature of humic acid increases. As a result, the access of humic acid to the active sites of the nanocomposite increases and the degradation of humic acid increases.

Effect of pH

The state of dispersion of positive and negative charges on the surface of the catalyst is one of the important factors that can affect the efficiency of the photocatalytic process. On the other hand, these conditions are a function of pHzpc and pH of the reaction medium. The effect of pH on the photocatalytic degradation efficiency of humic acid by $ZnFe_2O_4$@ZnO nanocomposites in the range of 3–11 is shown in Figure 10. At this stage, the pH of humic acid solution with a concentration of 30 mg/L and a concentration of 0.2 g/L of the synthesized nanocomposite was studied. The results of the effect of pH showed that the removal efficiency of humic acid by $ZnFe_2O_4$@ZnO nanocomposite increases with decreasing pH. The maximum removal of

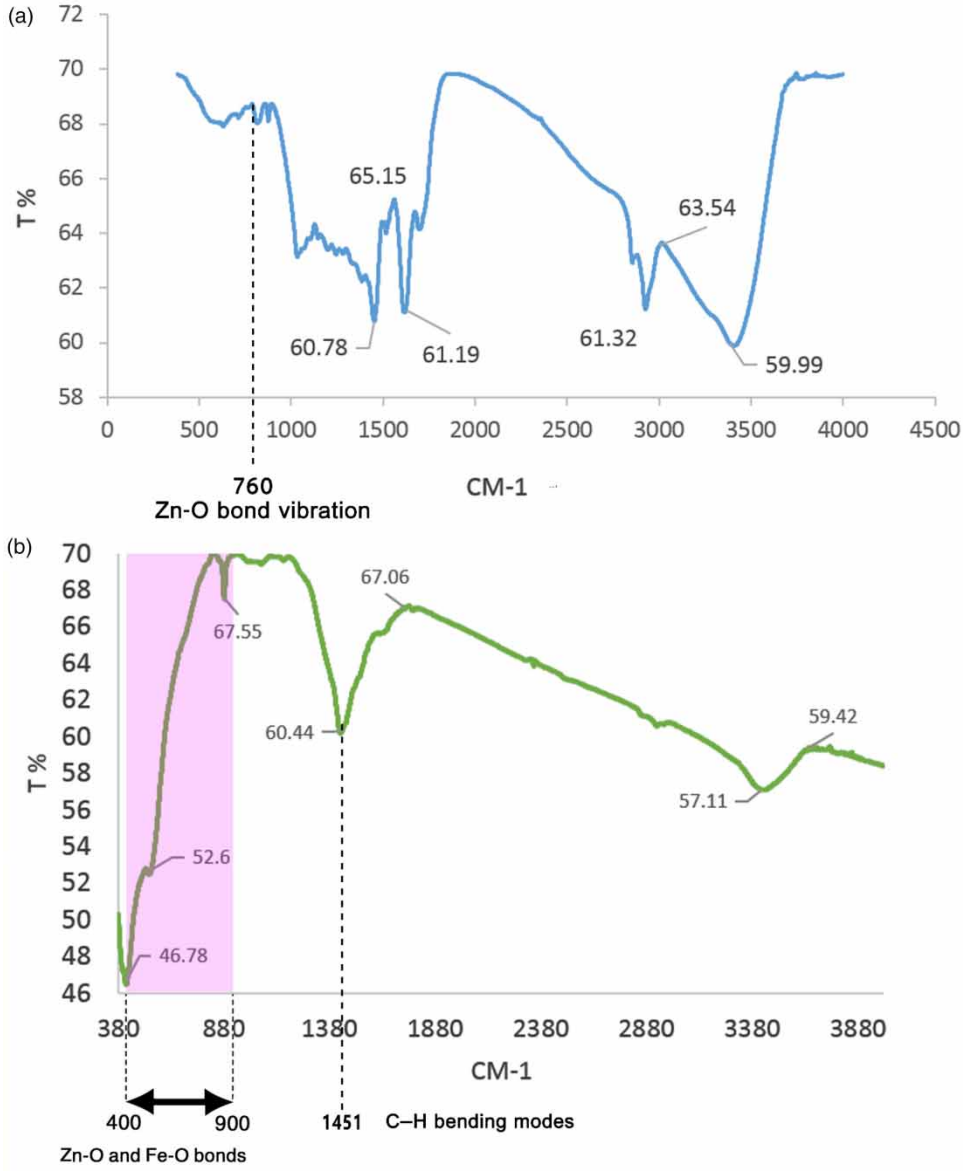

Figure 6 | FT-IR spectra of (a) $ZnFe_2O_4$ and (b) $ZnFe_2O_4$@ZnO.

humic acid occurred at pH = 3, which was chosen as the optimal pH. The reason for this can be attributed to the anionic nature of humic acid and pHzpc nanocomposite. Variation of the pH solution changes the surface charge of the catalyst particles and pollutant adsorption on the surface also changes the reaction rate. It can be expressed at acidic pH, humic acid diffuses faster (Doulia *et al.* 2009). In other words, the degradation of humic acid by $ZnFe_2O_4$@ZnO nanocomposite is inversely proportional to increasing pH. At lower pH values, humic acid molecules do not have to compete with the large number of H^+ cations in the solution for the surface sites of the nanocomposite and as a result, the destruction rate is relatively high. But in alkaline pH, hydrogen peroxide ions are produced. The electromagnetic repulsion force between humic acid and nanoparticles in alkaline pH is intensified due to the increased competition between humic acid anions and hydroxide ions to connect to active sites and degradation efficiency decreases (Tamimi *et al.* 2008; Kamranifar *et al.* 2019b; Sahoo & Hota 2019; Mohammadi *et al.* 2022). In a study, the removal of Congo red dye was performed with $ZnFe_2O_4$@ZnO nanocomposite, and the maximum removal efficiency was achieved on the surface of the nanocomposite in an acidic environment and decreased in an alkaline environment (Karamipour *et al.* 2016).

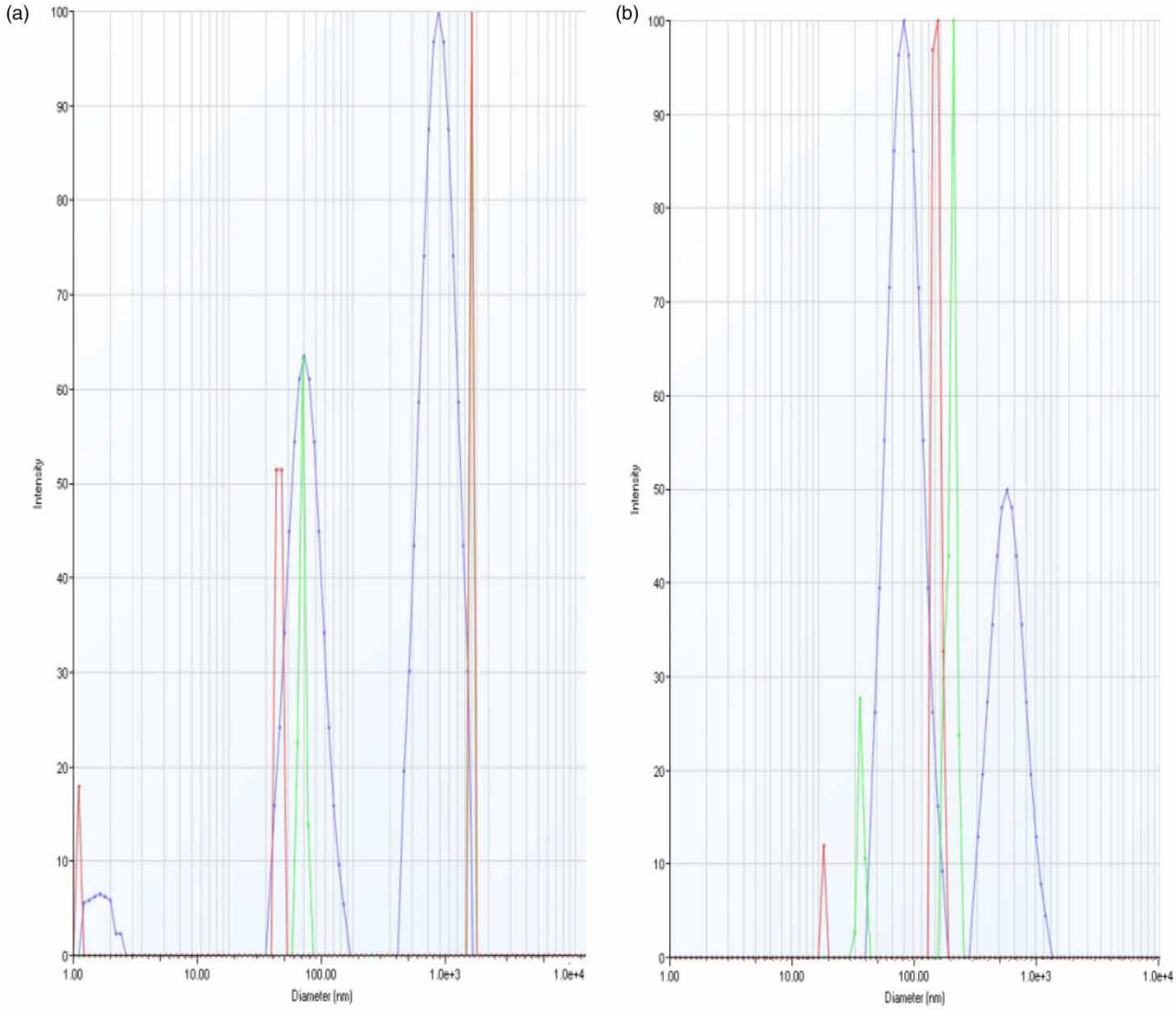

Figure 7 | DLS (dynamic light scattering) analysis of (a) $ZnFe_2O_4$ and (b) $ZnFe_2O_4$@ZnO nanoparticles.

Effect of catalyst dosage

The effect of catalyst dosage on the photocatalytic degradation of humic acid by $ZnFe_2O_4$@ZnO nanocomposite was investigated with nanocomposite concentrations ranging from 0.005 to 0.1 g/L (Figure 11). According to the obtained results, it was observed that initially, with the increase in the concentration of nanocomposite, the efficiency of the process in the degradation of humic acid increased, and the maximum amount of degradation of humic acid was in the concentration of nanocomposite 0.05 g/L, but with the increase in the concentration of nanocomposite to 0.1 g/L of nanocomposite, the rate of pollutant degradation has decreased, which can be related to the self-competitive reactions of nanocomposite in solution.

According to the locations of the catalyst surface and the amount of UVc light transmission, with increasing concentration up to 0.05 g/L, the number of active sites on the nanocomposite surface and the production of hydroxyl radicals and finally the degradation of humic acid increases. Also, the results showed that with the increase in the concentration of nanocomposite, their accumulation in the solution increases, and as a disruptive factor, by preventing the passage of ultraviolet light, the degradation efficiency decreases. Therefore, the concentration of 0.05 g/L of catalyst was chosen as the optimal

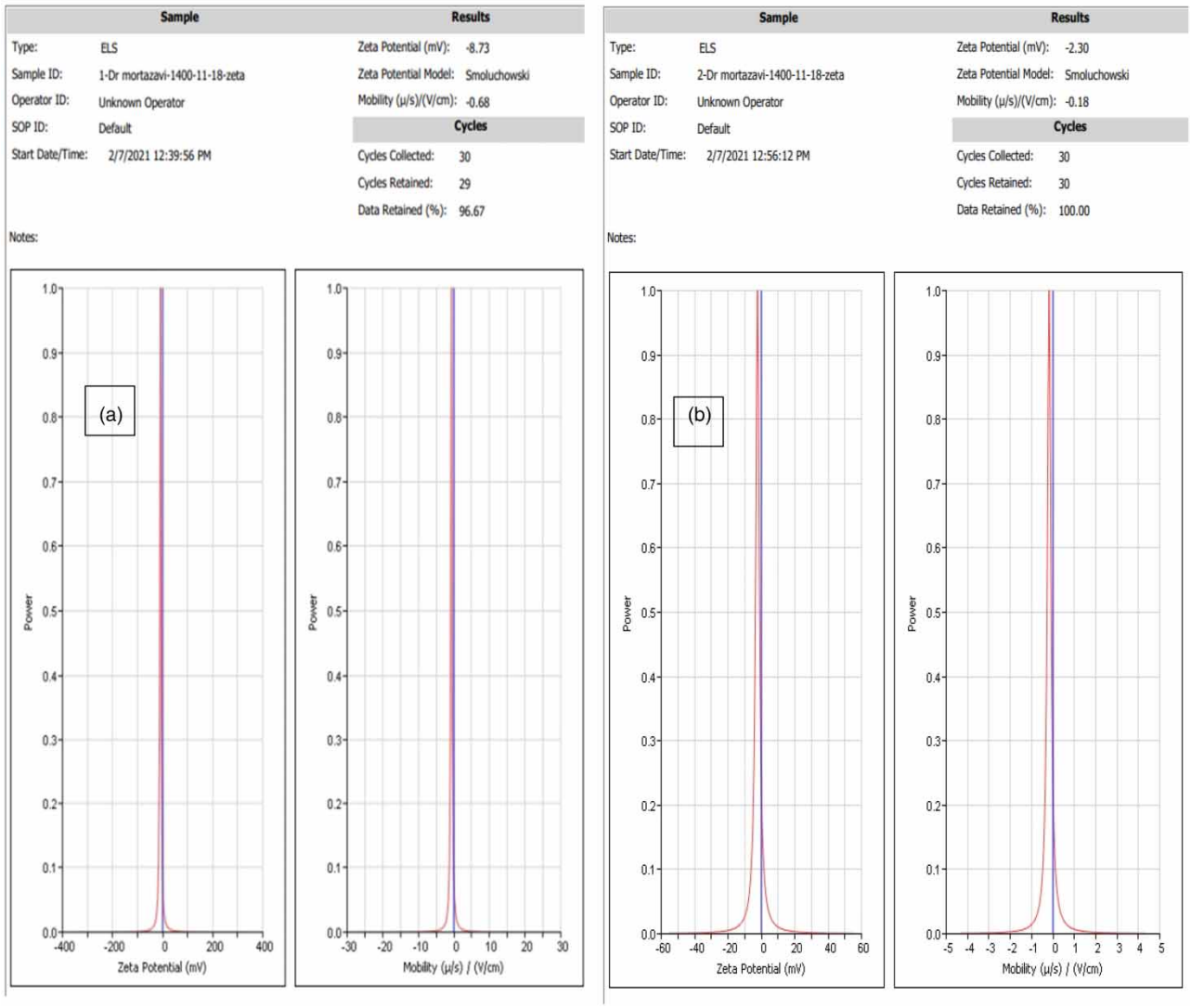

Figure 8 | Zeta potential values of (a) $ZnFe_2O_4$ and (b) $ZnFe_2O_4$@ZnO.

concentration for the next experiments. In the study of photocatalytic removal of humic acid by $MnFe_2O_4$@TiO_2 nanocomposite, it was shown that with increasing doses of nanocomposite, the rate of degradation of humic acid increased and then with increasing dose of nanocomposite pollutant degradation decreased again (Derakhshani & Naghizadeh 2022).

Effect of humic acid concentration

For this purpose, five solutions in different concentrations of 2–15 mg/L of humic acid were prepared and 0.05 g/L of $ZnFe_2O_4$@ZnO nanocomposite and pH = 3 were subjected to photocatalytic degradation. As shown in Figure 12, the degradation of humic acid decreased by increasing the concentration of humic acid up to 10 mg/L, and after increasing the concentration to 15 mg/L, the degradation increased.

The reason for the decrease in efficiency with the increase in humic acid concentration can be that at lower pollutant concentrations, active sites on the surface of the nanocomposite are more available for the absorption of humic acid. Increasing the concentration of humic acid as an intervention led to a decrease in the available sites of the nanocomposite and an increase in repulsive forces. Also, at the beginning of the process, the degradation of humic acid by the nanocomposite happened fast, and after that, the rate of degradation was slower, which can be explained by the fact that in the early stages of degradation, due to the complete availability of nanocomposite sites, the process was carried out faster. After the reduction of

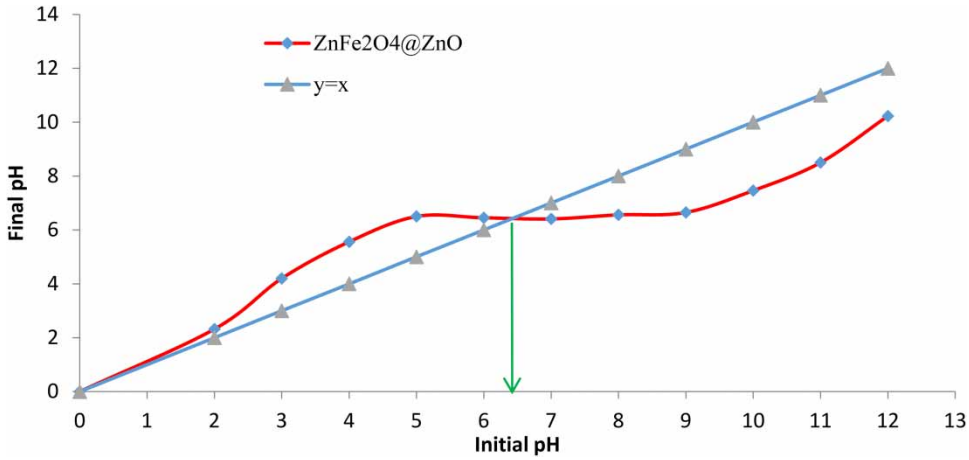

Figure 9 | pHzpc of magnetic $ZnFe_2O_4$@ZnO nanocomposite.

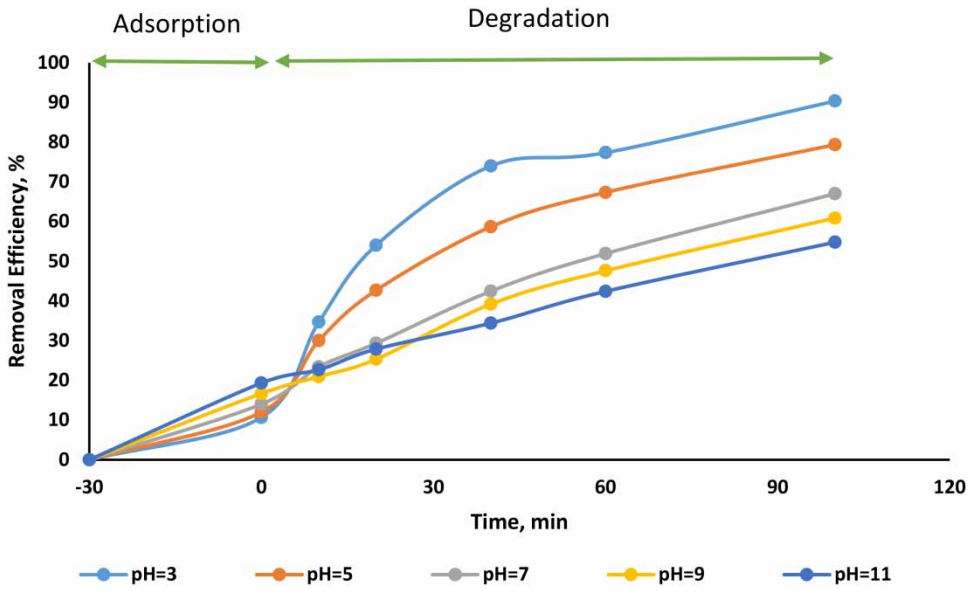

Figure 10 | Effect of pH in photocatalytic degradation of humic acid by $ZnFe_2O_4$@ZnO nanocomposite.

the mentioned sites, the degradation rate became a little slower, and on the other hand, the increase in the concentration of humic acid interferes and reduces the production of hydroxyl radicals. Another reason for this is the electron excitation of the catalyst produced by hydroxyl radicals in the early stages. But at the concentration of 15 mg/L, due to the increase in the mass driving force of the humic acid solution, more pollutant molecules were transferred to the surface of the $ZnFe_2O_4$@ZnO nanocomposite and the degradation increased (Farzadkia *et al.* 2015; Kamranifar *et al.* 2019a, 2019b; Nguyen *et al.* 2022).

Catalyst reusability and stability

Performing stability and reusability tests is one of the important factors in advanced oxidation photocatalytic processes. According to Figure 13, it was found that the $ZnFe_2O_4$@ZnO nanocomposite has an acceptable reusability and recovery after being tested in five stages without any significant reduction. And the slight reduction of nanocomposite is due to the reduction of mass during processes such as washing and drying as well as magnetic separation (Kamranifar *et al.* 2019a).

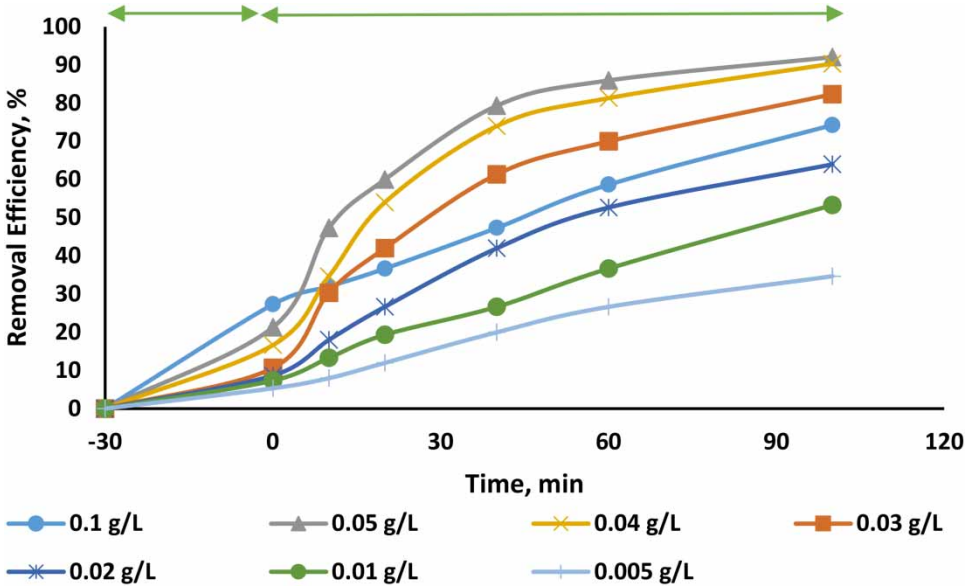

Figure 11 | Effect of catalyst dosage in photocatalytic degradation of humic acid by $ZnFe_2O_4$@ZnO nanocomposite.

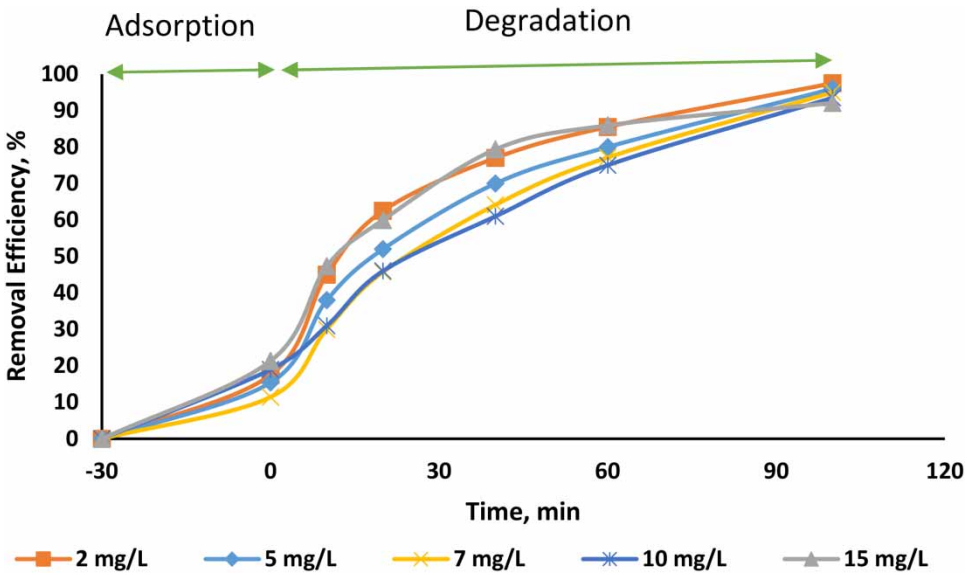

Figure 12 | Effect of humic acid concentration in photocatalytic degradation of humic acid by $ZnFe_2O_4$@ZnO nanocomposite.

Degradation mechanism of humic acid photocatalyst by $ZnFe_2O_4$@ZnO nanocomposite

Figure 14 shows the degradation mechanism of humic acid photocatalyst by $ZnFe_2O_4$@ZnO nanocomposite. The photocatalytic reaction can be explained with the help of different stages of oxidation and reduction. By ultraviolet light irradiation, $ZnFe_2O_4$ is excited and produces electrons and electron holes. These generated electrons are transferred to the ZnO conduction band and react with oxygen to produce super peroxide radicals and produce secondary substances. On the other hand, empty holes in $ZnFe_2O_4$ also react with hydroxyl groups and produce hydroxyl radicals, and finally, the chain reaction between electrons and holes increases the production of hydroxyl radicals, and as a result, it destroys pollutants on the nanocomposite (Zouhier *et al.* 2020).

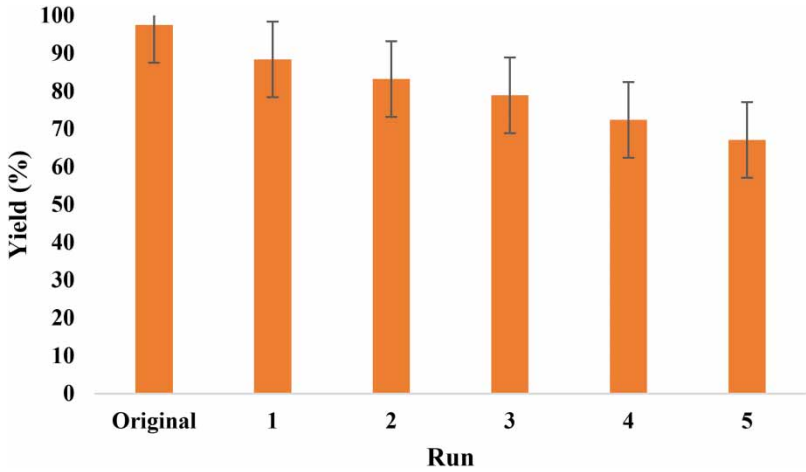

Figure 13 | The reusability of $ZnFe_2O_4$@ZnO nanocomposite in photocatalytic degradation of humic acid under optimum conditions.

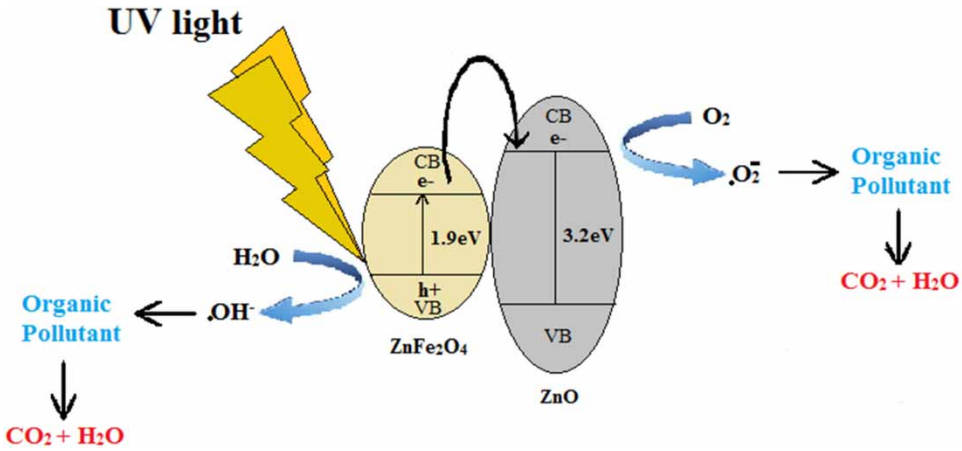

Figure 14 | Schematic of photocatalysis process of humic acid by $ZnFe_2O_4$@ZnO.

CONCLUSION

In this study, the photocatalytic degradation efficiency of humic acid using $ZnFe_2O_4$@ZnO nanoparticles was investigated in the presence of UV light. The green synthesized $ZnFe_2O_4$@ZnO nanoparticles were characterized with different analyses. Also, the effects of different parameters on the photocatalytic degradation process were investigated. The results of this study showed that the highest percentage of humic acid degradation by $ZnFe_2O_4$@ZnO nanocomposite was at pH = 3, the initial humic acid concentration of 15 mg/L and $ZnFe_2O_4$@ZnO nanocatalyst of 0.05 g/L. Also, after five stages of saturation and regeneration, this nanocatalyst still had a high capacity in humic acid degradation. Therefore, it can be said that this nanocomposite has a high ability to remove humic acid from water resources.

AUTHORS' CONTRIBUTIONS

M. A. wrote the draft of the paper. A. N. was the supervisor of this research project and contributed to conception and design of the work. A. H. and S. M. contributed to acquisition and analysis of the data. A. J. and F. M. contributed to substantively revise the work. All authors read and approved the final manuscript.

FUNDING

The authors declare that no funds, grants or other support were received during the preparation of this manuscript.

DATA AVAILABILITY STATEMENT

All relevant data are included in the paper or its Supplementary Information.

CONFLICT OF INTEREST

The authors declare there is no conflict.

REFERENCES

Agarwal, H., Kumar, S. V. & Rajeshkumar, S. 2017 A review on green synthesis of zinc oxide nanoparticles – an eco-friendly approach. *Resource-Efficient Technologies* **3**, 406–413.

Algamdi, M. S., Alsohaimi, I. H., Lawler, J., Ali, H. M., Aldawsari, A. M. & Hassan, H. M. 2019 Fabrication of graphene oxide incorporated polyethersulfone hybrid ultrafiltration membranes for humic acid removal. *Separation and Purification Technology* **223**, 17–23.

Amor, C., Marchão, L., Lucas, M. S. & Peres, J. A. 2019 Application of advanced oxidation processes for the treatment of recalcitrant agro-industrial wastewater: a review. *Water* **11**, 205.

Babu, D. S., Srivastava, V., Nidheesh, P. & Kumar, M. S. 2019 Detoxification of water and wastewater by advanced oxidation processes. *Science of the Total Environment* **696**, 133961.

Chianese, S., Fenti, A., Iovino, P., Musmarra, D. & Salvestrini, S. 2020 Sorption of organic pollutants by humic acids: a review. *Molecules* **25**, 918.

Derakhshani, E. & Naghizadeh, A. 2014 Ultrasound regeneration of multi wall carbon nanotubes saturated by humic acid. *Desalination and Water Treatment* **52**, 7468–7472.

Derakhshani, E. & Naghizadeh, A. 2022 Biosynthesis of MnFe(2)O(4)@TiO(2) magnetic nanocomposite using oleaster tree bark for efficient photocatalytic degradation of humic acid in aqueous solutions. *Environmental Science and Pollution Research* **30**, 3862–3871.

Doulia, D., Leodopoulos, C., Gimouhopoulos, K. & Rigas, F. 2009 Adsorption of humic acid on acid-activated Greek bentonite. *Journal of Colloid and Interface Science* **340**, 131–141.

Farzadkia, M., Bazrafshan, E., Esrafili, A., Yang, J. K. & Shirzad-Siboni, M. 2015 Photocatalytic degradation of Metronidazole with illuminated TiO_2 nanoparticles. *Journal of Environmental Health Science and Engineering* **13**, 35.

Geoprincy, G., Srri, B. V., Poonguzhali, U., Gandhi, N. N. & Renganathan, S. 2013 A review on green synthesis of silver nanoparticles. *Asian Journal of Pharmaceutical and Clinical Research* **6**, 8–12.

Ghernaout, D. & Elboughdiri, N. 2020 Advanced oxidation processes for wastewater treatment: facts and future trends. *Open Access Library Journal* **7**, 1–15.

Kamranifar, M., Allahresani, A. & Naghizadeh, A. 2019a Synthesis and characterizations of a novel $CoFe_2O_4$@ CuS magnetic nanocomposite and investigation of its efficiency for photocatalytic degradation of penicillin G antibiotic in simulated wastewater. *Journal of Hazardous Materials* **366**, 545–555.

Kamranifar, M., Masoudi, F., Naghizadeh, A. & Asri, M. 2019b Fabrication and characterization of magnetic cobalt ferrite nanoparticles for efficient removal of humic acid from aqueous solutions. *Desalination and Water Treatment* **144**, 233–242.

Karamipour, A., Rasouli, N., Movahedi, M. & Salavti, H. 2016 A kinetic study on adsorption of Congo red from aqueous solution by ZnO-$ZnFe_2O_4$-polypyrrole magnetic nanocomposite. *Physical Chemistry Research* **4**, 291–301.

Krishnan, S., Murugesan, S., Vasanthakumar, V., Priyadharsan, A., Alsawalha, M., Alomayri, T. & Yuan, B. 2021 Facile green synthesis of $ZnFe_2O_4$/rGO nanohybrids and evaluation of its photocatalytic degradation of organic pollutant, photo antibacterial and cytotoxicity activities. *Colloids and Surfaces A: Physicochemical and Engineering Aspects* **611**, 125835.

Li, X., Jin, B., Huang, J., Zhang, Q., Peng, R. & Chu, S. 2018 Fe_2O_3/ZnO/$ZnFe_2O_4$ composites for the efficient photocatalytic degradation of organic dyes under visible light. *Solid State Sciences* **80**, 6–14.

Lv, H., Ma, L., Zeng, P., Ke, D. & Peng, T. 2010 Synthesis of floriated $ZnFe_2O_4$ with porous nanorod structures and its photocatalytic hydrogen production under visible light. *Journal of Materials Chemistry* **20**, 3665–3672.

Matilainen, A. & Sillanpää, M. 2010 Removal of natural organic matter from drinking water by advanced oxidation processes. *Chemosphere* **80**, 351–365.

Moctezuma, E., Leyva, E., Aguilar, C. A., Luna, R. A. & Montalvo, C. 2012 Photocatalytic degradation of paracetamol: intermediates and total reaction mechanism. *Journal of Hazardous Materials* **243**, 130–138.

Mohammadi, N., Allahresani, A. & Naghizadeh, A. 2022 Enhanced photo-catalytic degradation of natural organic matters (NOMs) with a novel fibrous silica-copper sulfide nanocomposite (KCC1-CuS). *Journal of Molecular Structure* **1249**, 131624.

Nabi, G., Khalid, N., Tahir, M. B., Rafique, M., Rizwan, M., Hussain, S., Iqbal, T. & Majid, A. 2018 A review on novel eco-friendly green approach to synthesis TiO2 nanoparticles using different extracts. *Journal of Inorganic and Organometallic Polymers and Materials* **28**, 1552–1564.

Naghizadeh, A., Momeni, F. & Derakhshani, E. 2013a Efficiency of ultrasonic process in regeneration of graphene nanoparticles saturated with humic acid. *Desalination and Water Treatment* **70**, 290–293.

Naghizadeh, A., Nasseri, S., Mahvi, A. H., Kalantary, R. R. & Rashidi, A. 2013b Continuous adsorption of natural organic matters in a column packed with carbon nanotubes. *Journal of Environmental Health Science and Engineering* **11**, 14.

Naghizadeh, A., Nasseri, S., Mahvi, A. H., Nabizadeh, R. & Kalantary, R. R. 2015 Fenton regeneration of humic acid-spent carbon nanotubes. *Desalination and Water Treatment* **54**, 2490–2495.

Nguyen, L. T., Vo, D.-V. N., Nguyen, L. T., Duong, A. T., Nguyen, H. Q., Chu, N. M., Nguyen, D. T. C. & Van Tran, T. 2022 Synthesis, characterization, and application of $ZnFe_2O_4$@ ZnO nanoparticles for photocatalytic degradation of Rhodamine B under visible-light illumination. *Environmental Technology & Innovation* **25**, 102130.

Rabbani, M., Heidari-Golafzani, M. & Rahimi, R. 2016 Synthesis of TCPP/$ZnFe_2O_4$@ ZnO nanohollow sphere composite for degradation of methylene blue and 4-nitrophenol under visible light. *Materials Chemistry and Physics* **179**, 35–41.

Rameshbabu, R., Kumar, N., Karthigeyan, A. & Neppolian, B. 2016 Visible light photocatalytic activities of $ZnFe_2O_4$/ZnO nanoparticles for the degradation of organic pollutants. *Materials Chemistry and Physics* **181**, 106–115.

Sahoo, S. K. & Hota, G. 2019 Amine-functionalized GO decorated with ZnO-$ZnFe_2O_4$ nanomaterials for remediation of Cr (VI) from water. *ACS Applied Nano Materials* **2**, 983–996.

Sarathy, S. & Mohseni, M. 2006 An overview of UV-based advanced oxidation processes for drinking water treatment. *IUVA News* **8**, 16–27.

Shirzadi-Ahodashti, M., Ebrahimzadeh, M. A., Ghoreishi, S. M., Naghizadeh, A. & Mortazavi-Derazkola, S. 2020 Facile and eco-benign synthesis of a novel $MnFe_2O_4$@ SiO_2@ Au magnetic nanocomposite with antibacterial properties and enhanced photocatalytic activity under UV and visible-light irradiations. *Applied Organometallic Chemistry* **34**, e5614.

Stasinakis, A. 2008 Use of selected advanced oxidation processes (AOPs) for wastewater treatment – a mini review. *Global NEST Journal* **10**, 376–385.

Su, J., Shang, Q., Guo, T., Yang, S., Wang, X., Ma, Q., Guan, H., Xu, F. & Tsang, S. C. 2018 Construction of heterojunction $ZnFe_2O_4$/ZnO/Ag by using ZnO and Ag nanoparticles to modify $ZnFe_2O_4$ and its photocatalytic properties under visible light. *Materials Chemistry and Physics* **219**, 22–29.

Sun, L., Shao, R., Tang, L. & Chen, Z. 2013 Synthesis of $ZnFe_2O_4$/ZnO nanocomposites immobilized on graphene with enhanced photocatalytic activity under solar light irradiation. *Journal of Alloys and Compounds* **564**, 55–62.

Tamimi, M., Qourzal, S., Barka, N., Assabbane, A. & Ait-Ichou, Y. 2008 Methomyl degradation in aqueous solutions by Fenton's reagent and the photo-Fenton system. *Separation and Purification Technology* **61**, 103–108.

Tang, S., Tang, J., Yuan, D., Wang, Z., Zhang, Y. & Rao, Y. 2020 Elimination of humic acid in water: comparison of UV/PDS and UV/PMS. *RSC Advances* **10**, 17627–17634.

Wang, C., Tan, X., Yan, J., Chai, B., Li, J. & Chen, S. 2017 Electrospinning direct synthesis of magnetic $ZnFe_2O_4$/ZnO multi-porous nanotubes with enhanced photocatalytic activity. *Applied Surface Science* **396**, 780–790.

Yadav, N., Chaudhary, L., Sakhare, P., Dongale, T., Patil, P. & Sheikh, A. 2018 Impact of collected sunlight on $ZnFe_2O_4$ nanoparticles for photocatalytic application. *Journal of Colloid and Interface Science* **527**, 289–297.

Zouhier, M., Tanji, K., Navio, J., Hidalgo, M., Jaramillo-Páez, C. & Kherbeche, A. 2020 Preparation of $ZnFe_2O_4$/ZnO composite: effect of operational parameters for photocatalytic degradation of dyes under UV and visible illumination. *Journal of Photochemistry and Photobiology A: Chemistry* **390**, 112305.

First received 19 May 2023; accepted in revised form 3 July 2023. Available online 9 August 2023